IJPSR (2016), Vol. 7, Issue 6 **(Research Article)**

INTERNATIONAL JOURNAL OF PHARMACEUTICAL SCIENCES AND RESEARCH

Received on 15 February, 2016; received in revised form, 27 April, 2016; accepted, 26 May, 2016; published 01 June, 2016

NATURE'S RESPONSE TO INFLUENZA: A HIGH THROUGHPUT SCREENING STRATEGY OF AYURVEDIC MEDICINAL PHYTOCHEMICALS

Balkrishna Acharya [1, 2], Saradindu Ghosh[1] and Hemanth Kumar Manikyam [*1]

Patanjali Natural Coloroma Pvt. Ltd. [1], Haridwar, Uttarakhand - 249404, India
University of Patanjali [2], Haridwar, Uttarakhand - 249402, India

Key words:

H1N1; Drug Discovery; Phytochemical; Ayurveda.

Correspondence to Author:
Hemanth Kumar Manikyam

Research Head/ CEO operation
Patanjali Natural Coloroma Pvt. Ltd., Haridwar, Uttarakhand - 249404, India

Email: phytochem2@gmail.com

ABSTRACT: Inhibition of viral coating protein is an established therapeutic strategy for the treatment of many influenza treatment regimes. Although resistance to such inhibitors is common phenomena in different influenza treatment, such resistance can be averted by targeting coating proteins with phytochemicals. Swine Flu neuraminidase protein (H1N1) has been currently focused target for influenza inhibitor research. We used computational high throughput screening approach to identify novel phytochemical inhibitors from phytochemical knowledgebase. Our computational method used in this study is an integration of qualitative models obtained from consensus hydrated virtual screening protocols for H1N1 Neuraminidase 1 (N1) to identify the novel phytochemical inhibitors. Using the available N1 crystal structures in protein databank flexibility and hydration states were analyzed and validated. The three representative crystal structures with open and closed conformations with highly conserved waters were used to screened the phytochemical database and identified novel inhibitors, among them a first in class alkaloids inhibitor that have shown better affinity against neuraminidase protein over marketed drugs. Our studies suggest that this computational screening approach may be broadly applicable for identifying inhibitors with potential for treating H1N1.

INTRODUCTION: Influenza inhibitors have been identified for the treatment of various flu virus ailments [1, 2]. However, compensatory mechanisms diminish the long-term efficacy of these inhibitors[3]. Drug resistance is often observed in the clinic as rapidly evolving flu virus cells are able to avoid inhibition by a single targeted therapy through a variety of mechanisms [4]. The resistance of flu toward inhibitor-directed therapeutics is often accompanied by a distinct change in glycoside and coating protein network composition through adaptive evolution reprogramming, allowing the flu to elude effects of the drug and manifest resistance[5].

QUICK RESPONSE CODE

DOI: 10.13040/IJPSR.0975-8232.7(6).2699-19

Article can be accessed online on: www.ijpsr.com

DOI link: http://dx.doi.org/10.13040/IJPSR.0975-8232.7 (6).2699-19

An established strategy to improve the durability of clinical responses to targeted therapies is to simultaneously inhibit neuraminidase conserved region targeting. However, discovering neuraminidase inhibitors with an appropriate target profile has been challenging and necessitated the application of target specific therapies, which can pose major clinical development challenges [6–9]. We therefore sought a strategy to identify single agent phytochemical compounds with the ability to target influenza promoting pathways.

We chose to target neuraminidase (N1) part of the H1N1 among the other virulent strains *viz*: H1N2, H1N3, H1N7 etc.[10] The novel H1N1 strain (swine flu strain), first reported in Mexico in 2009, was termed so because it mainly infected the swine and displayed two main surface antigens, H1 (Hemagglutinin type 1) and N1 (Neuraminidase type1). The H1N1 flu has 8 stranded RNA; among them one strand is derived from human flu strains,

two from avian strains, and five from swine strains. Lately, neuraminidase inhibitors have been found to effectively treat H1N1 virus infection [11, 12]. Phylogenetically, these subtypes are classified into two groups: N1, N4, N5, and N8 subtypes (group-1) and N2, N3, N6, N7, and N9 subtypes (group-2) [15]. Neuraminidase helps in breaking the linkages between sialic acid and cellular glycoproteins, glycolipids thereby disrupting the cell wall [13, 14] Neuraminidase has a single polypeptide chain that comprises of six conserved polar amino acids, followed by hydrophilic, variable amino acids. Predominantly β-Sheets are present in secondary structure. While the residues involved in the catalysis are preserved in subtypes N1–N9, these two groups were also found to be structurally distinct, as revealed by the X-ray crystal structures[15].

Resistance to known inhibitors arises from mutations in or around the enzyme active site. By far the most common of these mutations, H274Y, restricts the inhibition of oseltamivir by displacing the pentyloxy group out of a hydrophobic pocket close to the active site [16-19] Other mutations, particularly E119V, E119G, and R292K can affect binding of both oseltamivir and zanamivir but arise much less frequently [20, 21] Drug resistance and environmental influences helped this adaptive mutation of the strains to promote its efficacy multiple times than normal [22]. Thus, neuraminidase is a promising drug target for the treatment of various influenza viruses. Interestingly, along with the small molecules some natural compounds have ability to be good lead molecules against various archetypal seasonal or pandemic ailments.

Ancient concept of Flu Fevers:

Ayurveda, the oldest Indian traditional and alternative medicine has been used for centuries for treating various diseases [44]. However, there is no prominent description of swine flu treatment available in scriptures but we have made an attempt to reread the concept of *Ojus* and *Jwara Chikitsa* (Treatment of fevers) as swine flu infection shares common clinical symptoms [45-48].

The present study was carried out tounderstand the flexibility of the binding pocket with the help of the available crystal structures of N1 protein and to evaluate them to select the representative crystals for the virtual screening protocol. Water in the binding pocket is always the direct competitor of the compounds that are binding to them.

Hence to increase the precision of the virtual screening, the stable or conserved waters were also evaluated. The final objective of our study is exhaustive screening of the phytochemicals mainly alkaloids and flavonoids as potent neuraminidase inhibitor which leads to the discovery of novel H1N1 neuraminidase inhibitors and a first in class alkaloid/flavanoid inhibitor using the hydrated representative crystal structures of N1.We suggest that this virtual screening protocol along with different biochemical assay to establish potency of those compounds can be helpful to identify and generate a large dataset of active phytochemical therapeutic compounds for identifying H1N1 inhibitors.

MATERIAL AND METHODS:

Molecular activity data and decoy datasets:

All the modeling studies were carried out using the 2015- 3 version of Schrodinger software. The activity data for the known H1N1 inhibitors was extracted from the Pubchemdatabase (January 26, 2016). 14unique active compounds were selected based on their IC50 values. These compounds were converted into 3D structures and generated their protonation states (biological pH), canonical tautomer and corrected their geometric configuration using Ligprep tool. Activity of the compounds was normalized with to pIC50. These compounds were used to validate the computational hypothesis by estimating enrichment and also to determine thresholds for significant docking interactions.

Decoy Set Generation:

The selected 14 H1N1 inhibitors were submitted for generating the decoy sets from the Directory of Useful Decoys, Enhanced (DUD-E) (26, 27). This generated 50–100 decoy compounds per submitted ligand SMILES. The decoys also prepared for their proper ionization states (pH of 7.2), tautomeric forms, using LigPrepdefault settings. These prepared decoys were mixed with 14 actives and the resulting 764 compounds were exported as structure data files and unique IDs were assigned

based on unique canonical structures to facilitate post-docking enrichment calculation.

Ensemble docking protocol:

Receptor Preparation:

From the large pool of the crystal structures of H1N1 available in the protein databank, the structures with resolution with less than 2.5 Å, with co-crystal inhibitors, without breaks in the binding site were selected for further analysis. All the structures were superimposed to understand the flexibility of the binding site. Based on the flexibility of the binding site three H1N1 co-crystal structures were selected from the Protein Data Bank (PDB). The two crystal structures with PDBID 4MJU and 4KS1 having open conformation but with unique Arg156 conformation and other protein 4KS4 with closed conformation were chosen as the representative structures for the docking studies. Overall, the selection criteria included the atomic resolution of the X-ray crystal structure, diversity in the co-crystal ligand scaffold and ligand interactions in the binding site. Further conserved waters were analyzed by superimposing all the high-resolution structures. Using consensus water script in Bio Luminate tool conserved waters found in/around the ligand binding sites of 70% of the superimposed structures (**Fig.1**). As shown in the figure 4water are conserved near the binding site but only two waters HOH 618 and 866 which are having hydrogen bonding with ligand and receptor were tested in the docking model evaluation.

Three crystal structures ofH1N1 protein structures were pre-processed using the protein preparation to assign bond orders and refine the structure including hydrogen bond optimization and constrained minimization [23]. Where needed, missing side chains were added using Prime [24, 25]. For each structure, one protein chain with the co-crystal ligand was kept, and water molecules were deleted beyond 5 A^o from heteroatom groups. In addition, the internal hydrogen bond network was optimized, followed by constrained energy minimization.

Docking Protocol:

For the three optimized protein structures grids based potentials were generated for the binding sites using Glide Grid Generation with default settings along with the rotatable bond settings for the OH and SH groups of the binding site amino acids. Compounds obtained via Lig Prep for all (H1N1 known active and decoy) compounds were docked against the prepared three crystal structures of neuraminidase proteins using Glide extra precision (XP) with the default settings, except writing out at most 5 poses per ligand representation and including 25 poses per ligand for post-docking minimization [28-30]. The docking scores were analyzed with default XP-pose viewer file on each unique ligand representation structure, the scores of all corresponding docking poses were aggregated; pose-aggregate scores of unique ligand representations (generated in Lig Prep) were aggregated by unique (original) compound structure (across ionization states and tautomers). Based on model evaluation results for all ligand representations, for the final results we used the top scores obtained across all levels; for each ligand structure this corresponds to the best pose for the best ligand representation in the best protein-docking model.

Re-docking of each co-crystal ligand into its corresponding structure active site validated our docking setup to generate models; in each case the co-crystal pose was reproduced with RMSD values <1.5 A^0. Further evaluation of the docking model cross docking of the ligands to other neuraminidase proteins structures in the presence and absence of water.

Evaluation of the virtual screening and characterization of predictions:

The docking method was evaluated by the receiver operating characteristic (ROC), enrichment factors (EF) and by correlation of aggregate docking scores and activity data using the known H1N1 inhibitors and the decoy dataset for individual and consensus models. The aggregate docking scores exhibited the best overall relation to reported activity. Sensitivity (S) is defined as true positive rate (TPR), specificity (SP) is true negative rate (TNR) and accuracy is the overall correct prediction rate [(TP + TN)/N]. The ROC is [S/(1-SP)], i.e. TPR over FPR. EF is [TP (subset)/n(subset)]/[P(total)/n(total)], i.e. the ratio of true positives detected in the subset divided by

the fraction of overall (total) positives. The known H1N1 inhibitors were clustered by maximum common substructure using Clustering script of Schrodinger [31]. Correlation coefficients were computed for aggregate docking scores versus median activity for all clusters.

Induced Fit Docking:

Binding sites for the initial Glide [37-40] (version 6.1, Schrödinger, LLC, New York, NY, 2013) docking phases of the Induced Fit Workflow (Induced Fit Docking protocol 2015-3, New York, NY, 2013) [61, 62] were calculated on the 4MJUstructure, considering the centroid of the co-crystallized ligand 27S or (5R,9R,10S)-10-(acetylamino)-2-2amino-4-oxo-9-(pentan-3-yloxy)-1-thia-3-azapiro-[4,5]deca-2,6-diene-7 carboxylic acid for neuraminidase1, from PDB code (4MJU) for grid generation.

In this case, cubic inner boxes with dimensions of 10 Å were applied to the proteins, and outer boxes were automatically detected. Ring conformations of the investigated compounds were sampled using an energy window of 2.5 kcal/mol; conformations featuring non-planar conformations of amide bonds were penalized. Side chains of residues close to the docking outputs (within 8.0 Å of ligand poses) were reoriented using Prime, and ligands were re-docked into their corresponding low energy protein structures (Glide Extra Precision Mode), considering inner boxes dimensions of 5.0 Å (outer boxes automatically detected), with resulting complexes ranked according to Glide Score.

Calculation of binding energies using MM/GBSA:

The binding free energy was calculated according to the Generalized Born Model and Solvent Accessibility method, using Prime MM/GBSA [37] (Prime version 2.1, 2009). Phytochemicals and reference ligands-docked neuraminidase structures were used for calculation of free energy of the ensemble structures. The binding free energy $\Delta G_{binding}$ was calculated using the following equation:

$$\Delta G_{binding} = E_{R:L} - (E_R + E_L) + \Delta G_{SA} + \Delta G_{Solv} \quad \text{.....(1)}$$

$$\Delta G_{Solv} = G_{solv.complex} - G_{solv.\ Protein} - G_{solv.ligand} \quad \text{.....(2)}$$

$$\Delta G_{SA} = G_{SA.complex} - G_{SA.protein} - G_{SA.ligand} \quad \text{.....(3)}$$

Where $E_R + E_L$ is the sum of energies of unbound ligand and receptor, and $E_{R:L}$ is the energy of the docked complex. ΔG_{SA} is the difference of surface area energy of the protein-ligand complex and the sum of surface area energies of protein and ligand individually. ΔG_{SOLV} is the difference in the GBSA solvation energy of the complex and summation of individual salvation energies of protein and ligand. Energies of the complex were calculated using the OPLS-2005 Atom force field [35] and GB/SA continuum solvent model.

Molecular dynamics simulations:

MD simulations of the docked complexes were accomplished using Desmond Molecular Dynamics system, with Optimized Potentials for Liquid Simulations (OPLS) all-atom force field 2005 [35-37]. The prepared protein molecules were solvated in the presence of explicit solvent on a fully hydrated model with TIP4P water model in an orthorhombic periodic boundary box (distance between box wall and protein complex was kept at 10 Å to avoid the direct interaction with its own periodic image) to generate required systems for MD simulations. The energy of prepared systems for MD simulations was minimized to 5000 steps maximum using the steepest descent method until a gradient threshold (25 kcal/mol/Å) was reached, followed by L-BFGS (Low-memory Broyden-Fletcher- Goldfarb Shanno quasi-Newtonian minimizer) until a convergence threshold of 1 kcal/mol/Å was met.

The default parameters in Desmond were applied for systems equilibration. The so equilibrated systems were then used for simulations at 300 K temperature and a constant pressure of 1atm, with a time step of 2fs. The long range electrostatic interactions were handled using Smooth Particle Mesh Ewald Method. Cutoff method was selected to define the short range electrostatic interactions. A cutoff of 9 Å radiuses (default), was used. All

atom (OPLS force field) explicit water molecular dynamics simulations were performed using the Desmond 2015.3software suite via Maestro 9.9 [32-34]. Molecular dynamics(MD) was run on the docked receptor ligand complexes for 50 ns. Simulation analysis was performed using the Desmond trajectory analysis software.

Hydrogen bond and hydrophobic interaction analysis:

The parameters defining the H-bonds between ligand and the protein complexes were as follows: acceptor-donor atoms distances less than 3.3 Å, hydrogen acceptor atom distances less than 2.7 Å and an acceptor-donor angle of 90° or more. Ligand-bound protease structures obtained from Glide and the MD-stabilized representative structures from Desmond were selected for carrying out interaction studies. A representative structure was prepared by averaging the coordinates of various frames extracted from the most stable region of the trajectory, which persisted until the end of the simulation run.

RESULTS:

Ensemble docking to predict novel Neuraminidase binders:

In contrast to many viral coating proteins, publicly available small molecule inhibition and binding data for neuraminidase (H1N1) are limited. However, co-crystal structures of N1 are available in the Protein Data Bank (PDB) allowing for an unbiased structure-based approach to predict flexibility neuraminidase active site hydrophobic pocket binding.

To understand the flexibility of the binding pocket upon binding of various ligands, all the high-resolution crystal structures with diverse ligands were superimposed. These are two distinct conformations observed in the neuraminidase-binding pocket (**Fig.2**). The large loop starting from Gln136and ending with Arg156extends into the binding site as a closed conformation that results in decrease in volume of the binding site. When this loop move away from the pocket as open conformation the volume of the pocket increase and accommodate the bulkier groups of the ligands at this position. Further in the open conformation of the binding pocket, the amino acid Arg156 side chain exhibiting different conformations and changing the pocket size in this region. To test our state of art virtual screening protocol and to cover conformational flexibility 3 crystal structures with PDB IDs 4FS1, 4FS4 and 4MJU were selected. As shown in the figure 3 the crystal structures 4FS4 and 4MJU are open conformations but having distinct Arg156 side chain conformations and 4FS1 is a closed conformation.

Analysis of conserved hydration states:

Desolvation of the guest (ligand) inside the binding pocket of the host (protein) at the hydrophobic region of the protein makes the complex thermodynamically stable and ligand exhibits higher affinity. However the water which are having strong hydrogen bond interactions with protein and ligand are very stable on comparison with bulk water and cannot be easily desolated by the ligand upon binding. During the docking these stable waters should be identified and retained for accuracy. To identify the conserved waters the 10 high-resolution neuraminidase crystal structures obtained from the protein databank were superimposed. The consensus waters among the 70% of the crystal structures were identified and shown in the **Fig.3**. As depicted from the figure there are five consensus water molecules are very close to the ligands. The water molecules are labelled for the PDB 4MJU.

The waters HOH 701 and 850 which are near the solvent exposer region and little far away from the binding site have less influence on the ligand binding. The three waters HOH 618, 866 and 868 are inside the pocket and very close to the bound ligand. These waters might be crucial for ligand binding and further analyzed the hydrogen bond interaction which makes the waters to gain enthalpy; the water molecules 618 and 868 were showing strong hydrogen interactions with binding site amino acids and ligand. Hence during the docking model evaluations there waters were retained and tested for the docking accuracy and enrichment

Docking Method Validation:

Docking validation was performed not only to understand how docking protocol reproduces the

co-crystal conformation but also the effect flexibility and hydrations states of the binding site on docking reproducibility. Seven prepared crystal structures with high resolution having open and closed conformations were selected for docking validation. Docking studies was performed for each PDB using Glide extra precision (XP). Glide isa semi flexible docking method to predict multiple ligand binding poses and allocates a score to each pose by appraising binding affinity, incorporating several energetic terms and empirical parameterization [28-30].

Self-docking and cross docking of the co-crystal ligands in the absence and presence of the important conserved waters molecules. The co-crystals ligands docked into their corresponding crystal structures and also into the remaining crystal proteins to reproduce the co-crystal pose. The Table 1 shows RMSD values of self-docking and cross docking results for the seven crystal structures. The PDBIDs with 4MJU, 4KS4 and 4KS5 are open conformations and 4KS1, 4KS2, 4KS3 and 3TI3 are closed conformations. The RMSD values for all the proteins self-docking results (diagonal values) were unacceptable (>2.5A^0) except 4KS3 and 4KS4 that were having <2.5 A^0 RMSD values. The total average of RMSD for both the open and closed conformations of the self-docking is 2.892A^0. Moreover the average RMSD for cross docking values of each crystal structure is very high (>4A^o).

This clearly illustrates that self-docking and cross docking is not showing good reproducibility for the proteins without water. The similar studies were conducted in the presence of the important conserved waters (HOH 618 and 866) in the binding site. The RMSD values for the hydrated docking results were shown in the table 1. The reproducibility of the self- docking was greatly improved and the average RMSD is 1.63 A^0 for all the proteins. The reproducibility of the self-docking of all the proteins are less than >2.5A^0 accept for the 3TI3 protein.

Even for the cross docking the average RMSD for each protein improved significantly. The open conformation proteins able to reproduce co-crystals of closed conformations accurately not *vice versa.* The protein 4KS5 is showing the highest reproducibility (RMSD 2.5 A^0) followed by 4KS4. However the reproducibility of the open conformation co-crystal 27S (co-crystal of 4MJU) either by 4KS5 and 4KS4 is not precise this is due to conformational changes in the side chain of the Arg156 of 4MJU protein. Among the closed conformation proteins, 4KS3 is showing highest reproducibility of average RMSD of 2.945 A^0 for all the proteins and finest reproducibility for the closed co-crystal ligands. The results suggest that hydrated 4KS5 and 4MJU from the open conformation and 4KS3 from closed conformation will cover the flexibility of the neuraminidase 1 protein and selected for the virtual screening protocol.

Evaluation of Virtual Screening:

To maximize accuracy of the virtual screening using ensemble docking approach three crystal structures 4MJU, 4KS5 and 4KS3 was selected based on the docking reproducibility. However the success of the virtual screening mainly depends on how well the N1 docking protocol selects the actives from large database with minimal false positives. Hence the ensemble docking protocol was evaluated by screening the know database and calculated the hit rate using the enrichment and receiver operating characteristic (ROC).For the validation 14 known actives extracted from Drug Bank and 750 corresponding decoy compounds obtained from the Directory of Useful Decoys [26, 27] were assorted to generated know database (details described in Methods).

The known database was screened with three N1 proteins and pooled and computed sensitivity (true positive rate) and specificity, enrichment factors and ROC score of the docking model. The docking score cutoff of was ≤ -6, (smaller is better) with approximately±2 standard deviations from the mean distribution. For enrichment active compounds defined as plog P (p Activity) ≥ 6, with all others deliberated inactive and predicted active docking score $\leq -6$with N1 crystal structures. Evaluating the docking model presentation at a docking score threshold of ≤ -6 gave high sensitivity indicating that the model was good to classify active molecules appropriately, also the model was very specific to evaluate the known and

decoy compounds at docking score threshold of ≤ −6 (**Fig 5**). Enrichment factors calculated at 0.1 and 1% of the top docked compounds were high at the p Activity ≥ 6 activity thresholds (**Table 2**). The receiver operating characteristic AUC (ROC score) was outstanding for this activity cutoff, further supporting the models predictive performance (**Fig.5, Table 3**).These statistical cross validation results confirm very high quality of the consensus docking data model and the applicability for computer-generated selection. In addition to ROC scores and enrichment factors we also investigated how the collective docking scores and reported p Activity values relate quantitatively. As can be expected, there is not any comprehensive correlation, because docking scores appraised for relative binding affinity and typically cannot be related across diverse binding modes (**Fig. 6**). However, after clustering known N1 actives by maximum common substructure and topological features, we establish decent correlation for preserved chemo types. Pearson correlation coefficients (R^2) in the range of 0.4 to 0.9 were observed for active compounds, which include some recently marketed compounds(**Fig.7**).

We applied this N1 ensemble docking protocol to score the 30 compounds filtered from Ayurveda Shastra using the N1 activity classifiers and physicochemical properties. Compounds were then selected based on N1 docking score, physicochemical properties, chemical diversity and manual review. Our docking study of N1 inhibitors showed these compounds did extremely well in docking scores for further prioritization and testing (**Table 4, Fig.4A-4I**).

IFD result:

To testify the supposed conformational variations of the receptor's binding site cavity upon ligand binding, we employed the Induced Fit docking protocol [41, 42] (as implemented in the Schrödinger software package). Molecular modeling resulted in decent ccommodation of the explored alkaloids within the hydrophobic binding site of 4MJU, mainly packing between the hydrophobic residues (Asp 151, Arg118, Arg 371, Lys 430, Glu 432). We observed different conformations of compound rutin, aloe emodin and reference zanamivir within the 4MJU cavity, with the two functions pointing to the top of the pocket (**Fig.8**). Reference compound 27S was also found in orienting its primary binding mode towards the conserved Arg118 and Arg 37 (**Fig. 8**). In all cases the ligand poses resulted in promising predicted binding energy values (−9.791 kcal/mol for rutin, −9.168 kcal/mol for aloe emodin, and −8.73 kcal/mol for zanamivir). Induced fit docking study corroborated with our ensemble docking study generated models which showed the precision of the data aggregation (**Fig 9**). We identified in our calculations, in the case of compound rutin and aloe emodin, poses that exposed the functional groups towards the solvent may be further optimized based on its topology within the N1 binding site. To better understand the binding mode of the alkaloid scaffold to N1, given the multiple docking conformations observed, we thought to methodically investigate the topology of these fragments employing binding energy assay and molecular dynamics.

MMGBSA result:

In order to validate the accuracy of those docking, their binding free energy was correlated with docking score. The binding free energy inhibitors with N1 were calculated using the Prime/MM-GBSA post docking scoring protocol. Concisely, many energy modules, which contribute to binding energy were calculated for the complex holoenzyme, apoenzyme and free ligand binding energy was intended as the sum of difference between energy of complex holoenzyme and sum of energy of apoenzyme and free ligand. The calculated average free energies (ΔG_{bind}) results from different docking models are summarized in (**Table 5**). Interestingly, Prime/MM-GBSA predicted binding energy (ΔG_{bind}) could clearly distinguish with docking score between docking models.

Characterization of neuraminidase inhibitors by molecular dynamics:

To characterize how rutin and aloe emodin binds to 4MJU at the atomic level and gain insights into binding dynamics, we performed a 50 nanosecond (ns) molecular dynamics (MD) simulation (see Methods). The overall progress of the rutin and aloe emodin ligand may be compared via their Cα RMSDs versus time (**Fig. 10A** and **10B**).For aloe emodin Cα RMSD increased steadily over the first

20 ns or so and then plateau achieved around 22ns where as rutin Cα RMSD increases steadily over the first 20 ns or so and then plateaus up-to 50 ns. This suggested that substantial changes in the structure of the aloe emodin and rutin over the course of the 20ns time frame. In contrast, the C*α* RMSD for the protein receptor reached a peak destabilization around 8 ns for aloe emodin complex and around 18 ns for rutin complex then in both cases settled between 18 ns to 50 ns. This suggested that receptor had substantially smaller structural drift in comparison to ligands, thus that the complexes were stable structures. The protein RMSF (**Fig. 11A** and **11B**) gave us insights on how ligand fragments interact with the protein and their entropic role in the binding event.

The 'Fit Ligand on Protein' line showed the ligand fluctuations (fig 10A and 10B), with respect to the protein. The protein-ligand complex is first aligned on the protein backbone and then the ligand RMSF is measured on the ligand heavy atoms. Protein secondary structure elements (SSE) like alpha-helices and beta-strands were monitored throughout the simulation. The plot (**Fig. 12A** and **12B**) reported SSE distribution by residue index throughout the protein structure for aloe emodin-neuraminidase and rutin-neuraminidase complexes. The plot summarized the SSE composition for each trajectory frame over the course of the simulation, and the plot (**Fig. 13A** and **13B**) monitored each residue and its SSE assignment over time of simulation for aloe emodin and rutin complexes respectively.

The plot (**Fig. 14A** and **14B**) showed aloe emodin and rutin residues interaction with the protein in each trajectory frame. Some residues made more than one specific contact with the ligand, which was represented by a darker shade of orange, according to the scale to the right of the plot. Protein-ligand interactions (or 'contacts') of aloe emodin and rutin (**Fig. 15A** and **15B**) were categorized into four types: Hydrogen Bonds, Hydrophobic, Ionic and Water Bridges. Each interaction type contained more specific subtypes, which can be explored through the 'Simulation Interactions Diagram' panel. The stacked bar charts are normalized over the course of the trajectory: for example, a value of 0.7 suggests that 70% of the simulation time the specific interaction is maintained. Values over 1.0 are possible as some protein residue may make multiple contacts of same subtype with the ligand. Simulation analysis showed a conserved pi cataion interaction between aromatic ring of aloe emodin and Arg 118 (the conserved hydrophobic binding motif) and hydrogen bond with Glu227, and Arg 156 (**Fig.16A**). While this primary interaction was taking place, protein and ligand RMSD values stayed relatively low, indicating a stable binding conformation (**Fig. 10A**). However, from 0 to 22 ns, an increase in ligand RMSD is observed as the ligand switches its primary interaction to Arg 118 through a romatic stacking connections, destabilized the complex.

After 22 ns, the compound returns to its original binding con formation and re-established the binding connections observed before and remain same throughout the remaining time, with additional interactions observed with Glu 227 and Arg 156 (**Fig. 16A**). Simulation analysis also showed a hydrogen bond with Glu 432, Gly 147, Arg 118, Val 149 and Thr 439 (**Fig.16B**). While this primary interaction was taking place, protein and ligand RMSD values remained moderately low, indicating a stable binding conformation (**Fig.10B**). However, from 0 to 20 ns, an increase in ligand RMSD is observed as the ligand switches its primary interaction to Arg 118 through water bridge interactions, destabilizing the complex. After 20 ns, the compound returns to its original binding conformation and re-stabilizes the binding interactions observed previously throughout the remaining time, with additional interactions observed with Glu 432, Gly 147, Val 149 and Thr 439 (**Fig. 16B**).Two different crystal structures of the N1 from the protein data bank were taken to construct docking models (see Methods). The top docking score of Alo-emodin and Rutin in the N1 (− 9.168 kcal/mol and -9.71 kcal/mol) supports its observed high affinity. These results are also consistent with the MD simulation.

Docking pose and MD results clearly show Rutin and aloe emodin as a type I neuraminidase inhibitor due to its binding contacts with Arg118 in the active conformation of the N1 hydrophobic pocket domain activation loop. MD results show stable

RMSD values of Rutin and Aloe-emodin throughout the entire 50ns simulation. Throughout the time series Rutin and Aloe emodin interacted with all residues associated with hydrophobic pocket on average more than 75% of the time. Aloe emodin and Rutin molecule torsion angle panel showed the 2d schematic of a ligand with color-coded rotatable bonds. Dial (or radial) plots designate the conformation of the torsion throughout the course of the simulation (**Fig. 17A** and**17B**). The beginning of the simulation is in the center of the radial plot and the time evolution is plotted radially outwards. Ligands showed significant stability on structural conformation. The ligands properties histograms (**Fig. 18A** and **18B**) illustrated the conformational strain it undergoes to maintain a protein-bound conformation.

DISCUSSION: Inhibition of influenza promoting protein is an established therapeutic strategy for the treatment of various flu infections. Two inhibitors are approved for use in humans and few more are in clinical development. Computational designing of this kind of selectively unselective leads that bind to the desired disease targets, but avoid off-target liabilities is very difficult due to the high adaptive evolutionary change in viral proteins across the human populace. It is likely that most of the approved anti-influenza drugs are marginally striking the balance favorably. In contrast, it may be hard to optimize natural or nature derived phytochemical inhibitors, and there is strong evidence that such compound scan revel satisfactory effectiveness and pharmacology.

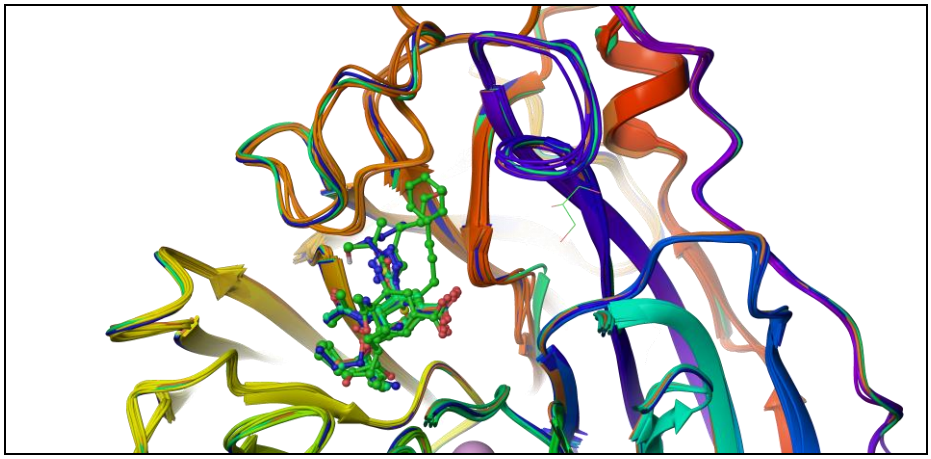

FIG.1: SUPERPOSITION OF NURAMINIDASE 1 CRYSTAL STRUCTURES HAVING DIFFERENT LIGANDS

We built distinct docking modelsafter picking three representative co-crystal structures, considering co-crystal ligand chemical diversity, quality and resolution of the structure and importantly the flexibility of the binding sites.

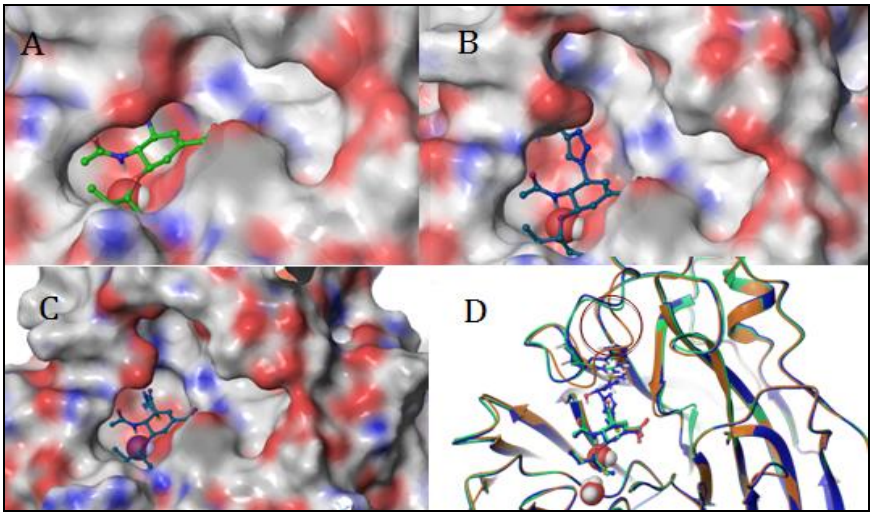

FIG.2: A. THE CLOSED CONFORMATION OF NEURAMINIDASE 1 (4KS1); B. OPEN CONFORMATION OF NEURAMINIDASE 1 (4KS4); C. OPEN CONFORMATION OF NEURAMINIDASE 1 WITH DISTINCT CONFORMATION OF ARG156 IN BINDING SITE D. SUPERIMPOSED STRUCTURES OF THE THREE CRYSTAL STRUCTURES (4MJU IN GREEN, 4KS1 IN BLUE AND 4KS4 IN BROWN) AND THE CIRCLE PORTION SHOWS THE CONFORMATIONAL CHANGES FROM CLOSED TO OPEN FORM.

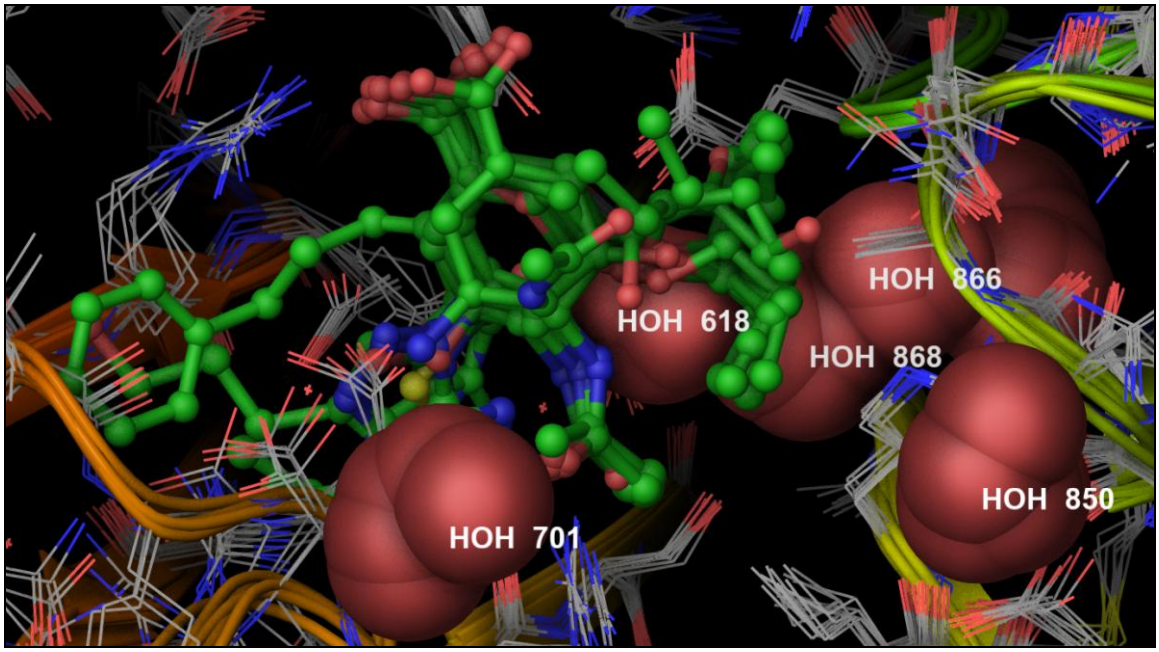

FIG.3: THE CONSENSUS WATERS REPRESENTED IN RED COLOR BALLS FOR THE SUPERIMPOSED H1N1 NEURAMINIDASE CRYSTAL STRUCTURES. THE LABELING OF THE WATERS IS SHOWN FOR THE PROTEIN 4MJU.

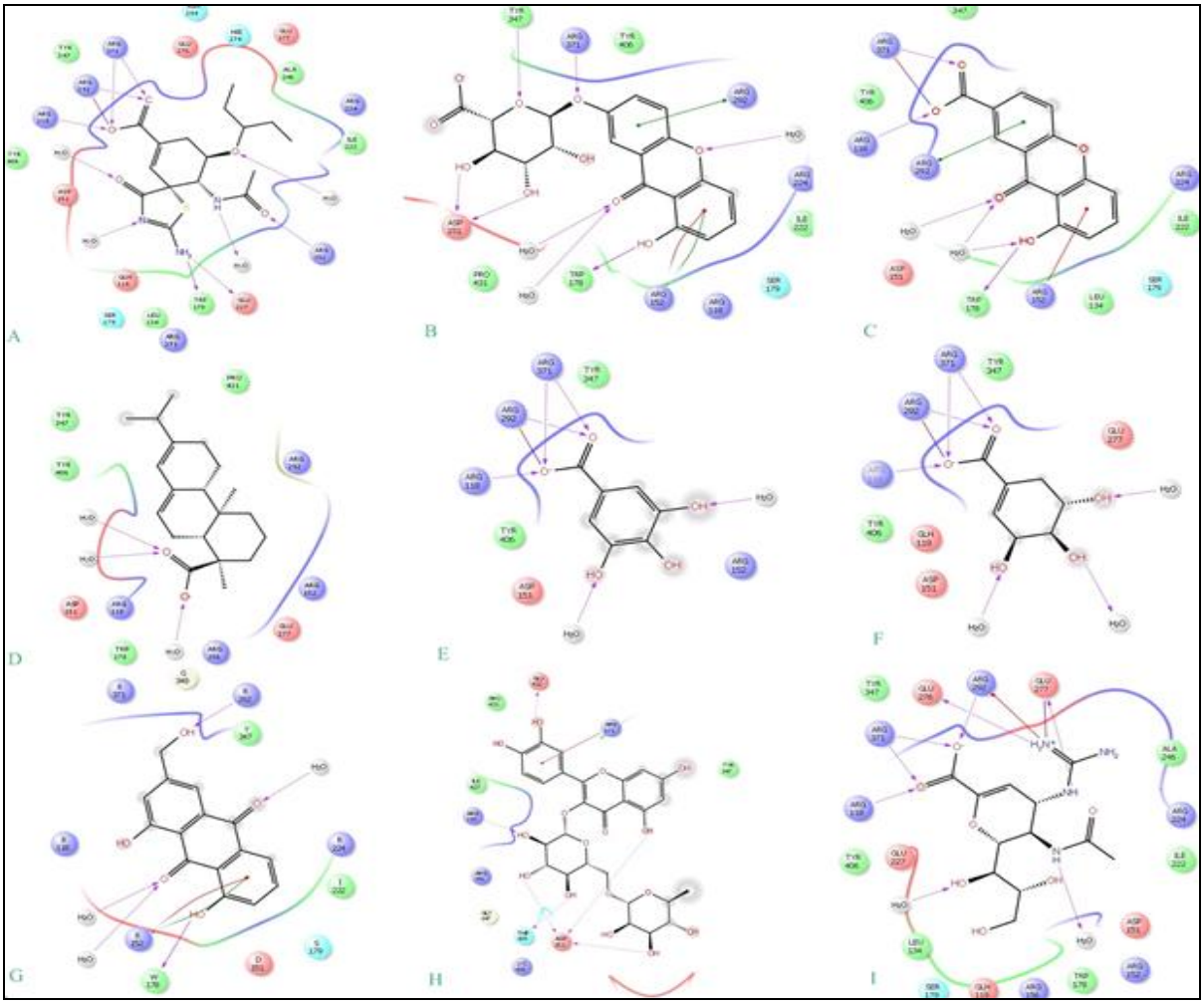

FIG. 4: THE ABOVE FIGURE 1ILLUSTRATES THE BINDING OF REPRESENTATIVE LIGAND STRUCTURE OF DIFFERENT PHYTOCHEMICALS AND KNOWN NEURAMINIDASE INHIBITOR WITH RECEPTOR 4MJU. IT ENLISTS A: 4MJU CO- CRYSTALLED COMPOUND 27S, B: EUXANTHIC ACID, C: ABEITICACID, D: GALLICACID, E: PRTOCATECHMIC ACID, F: SHIKIMIC ACID, G: ALOE EMODIN, H: RUTIN, I: ZANAMVIR.

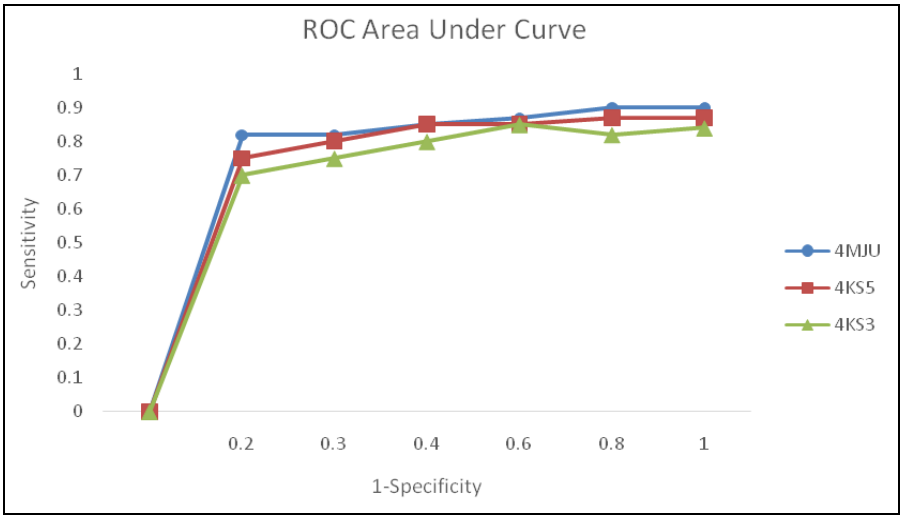

FIG. 5: ILLUSTRATES THE ENRICHMENT OF THE DECOY DATASET OF 764 COMPOUNDS AGAINST 4MJU, 4KS5 AND 4KS33 DOCKING MODELS. 4MJU, 4KS5 AND 4KS3 GENERATED AUCS WERE 0.93, 0.86 AND 0.82, RESPECTIVELY WHEN ITS BEDROCK VALUES WERE 0.88, 0.84 AND 0.80.

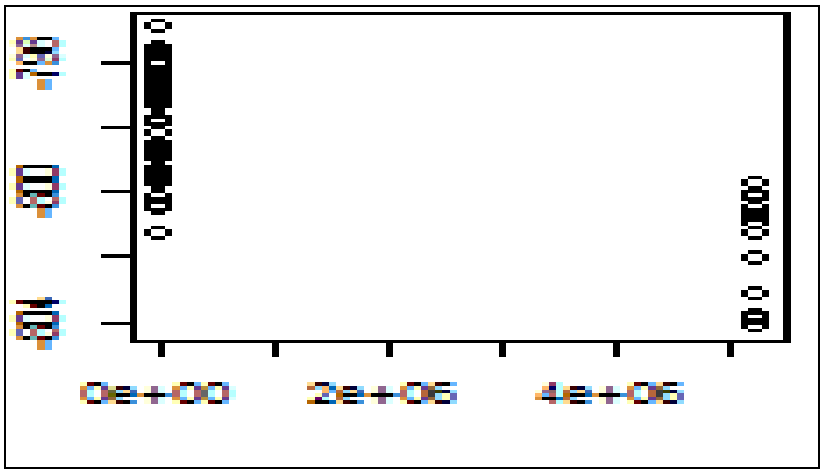

FIG. 6: ILLUSTRATES CORRELATION BETWEEN DOCKING SCORES AND LOG VALUE OF ACTIVITY DATA OF 764COMPOUNDS AGAINST 4MJU, 4KS5 AND 4KS3 DOCKING MODELS. THESE PROPERTIES ARE NOT CORRELATED WHICH IN TURNS SHOWED THAT GLOBAL CORRELATION OF DOCKING SCORE AND ESTIMATED RELATIVE BINDING AFFINITY MAY NOT BE POSSIBLE THROUGH NORMAL DOCKING PROCESS.

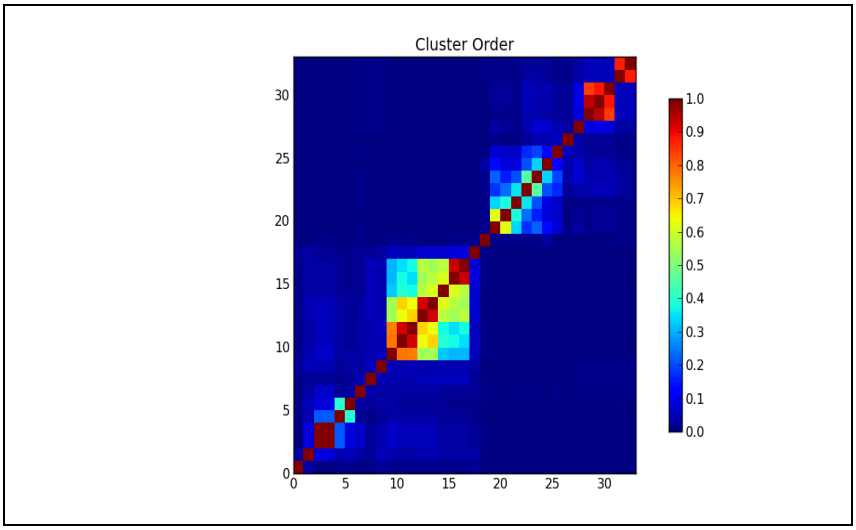

FIG. 7: ILLUSTRATES CLUSTERING OF KNOWN N1 ACTIVES BY MAXIMUM COMMON SUBSTRUCTURE AND TOPOLOGICAL FEATURES, WE FOUND GOOD CORRELATION FOR CONSERVED CHEMOTYPES. PEARSON CORRELATION COEFFICIENTS (R^2) IN THE RANGE OF 0.4 TO 0.9 WERE OBSERVED FOR ACTIVE COMPOUNDS, WHICH INCLUDE SOME RECENTLY MARKETED COMPOUNDS.

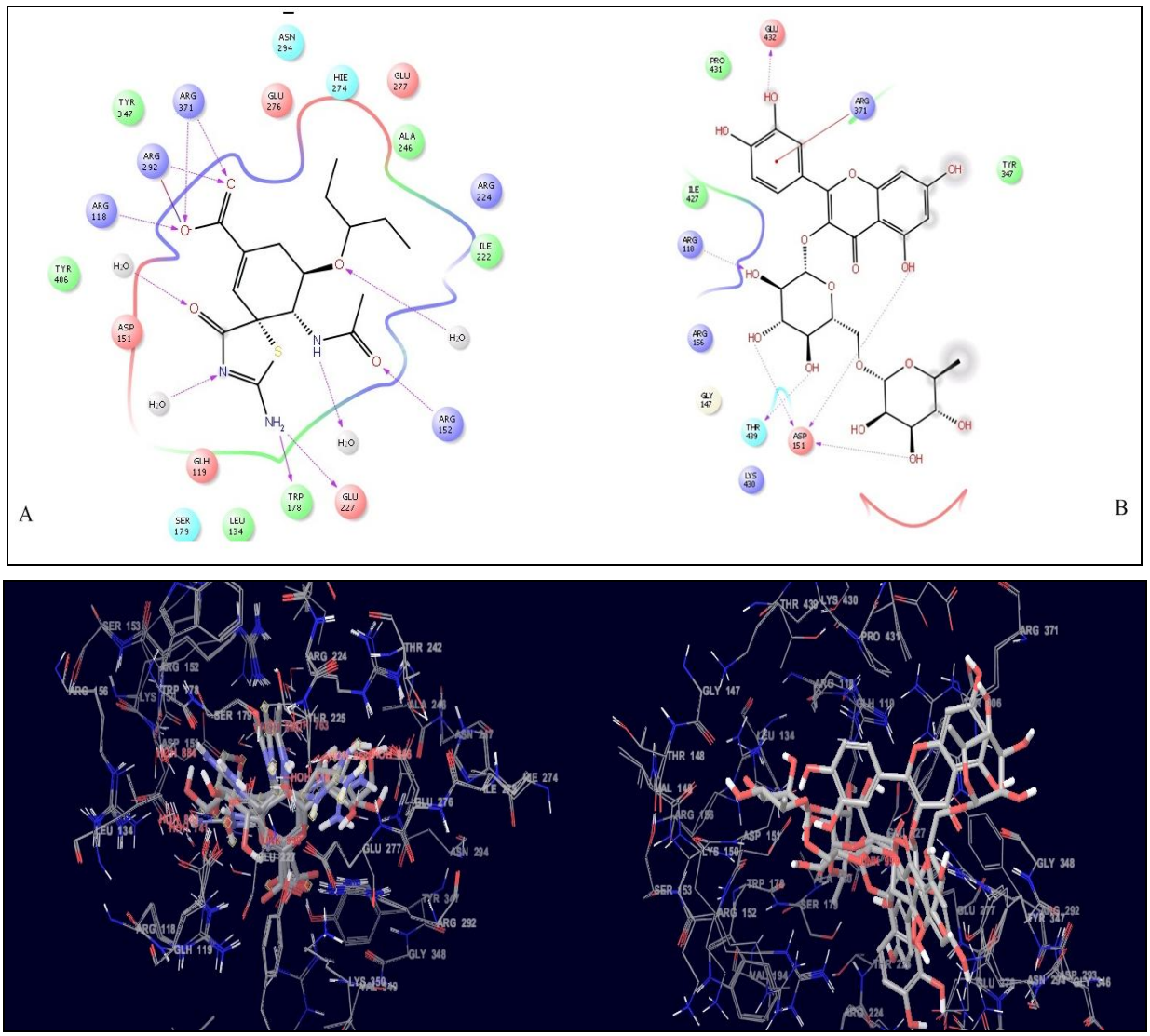

FIG.8: THE ABOVE FIGURE 8A, ILLUSTRATES THE BINDING OF REPRESENTATIVE ZANAMVIR LIGAND STRUCTURE WITH RECEPTOR 4MJU. IT SHOWS THE EXISTING HYDROGEN BONDS BETWEEN LIGAND AND RECEPTOR. IN PICTURE IT'S EVIDENT THAT THE REPRESENTATIVE LIGAND STRUCTURE BINDS WITH ARG 152, GLU 227, TRP 178, ARG 371, ARG 292, ARG 118 BY HYDROGEN BOND WHEREAS IN FIGURE 8B RUTIN FORMS PI-CATION INTERACTION WITH ARG 371 AND HYDROGEN BONDS WITH ARG 118, GLU 432, ASP 151, THR 439.

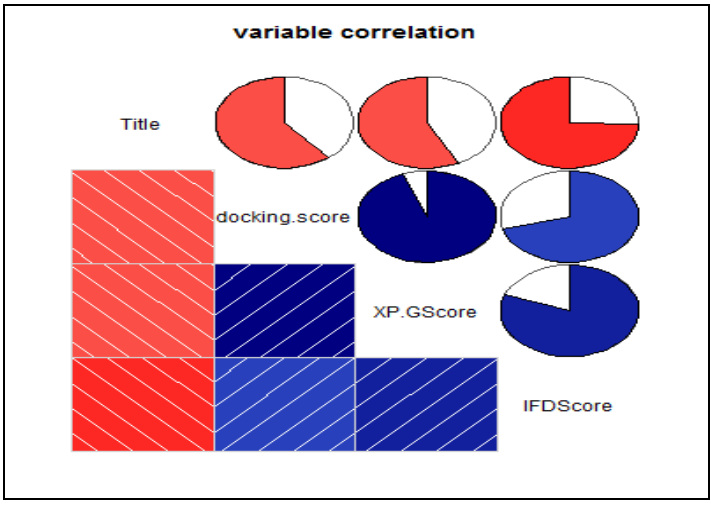

FIG. 9: ILLUSTRATES THAT INDUCED FIT DOCKING STUDY CORROBORATED WITH OUR ENSEMBLE DOCKING STUDY GENERATED MODELS WHICH SHOWED THE PRECISION OF THE DATA AGGREGATION. IFD SCORE, XP GSCORE AND DOCKING SCORE SHOWED 0.93, 0.84 AND 0.75 R^2 VALUES WITH EACH OTHER'S RESPECTIVELY.

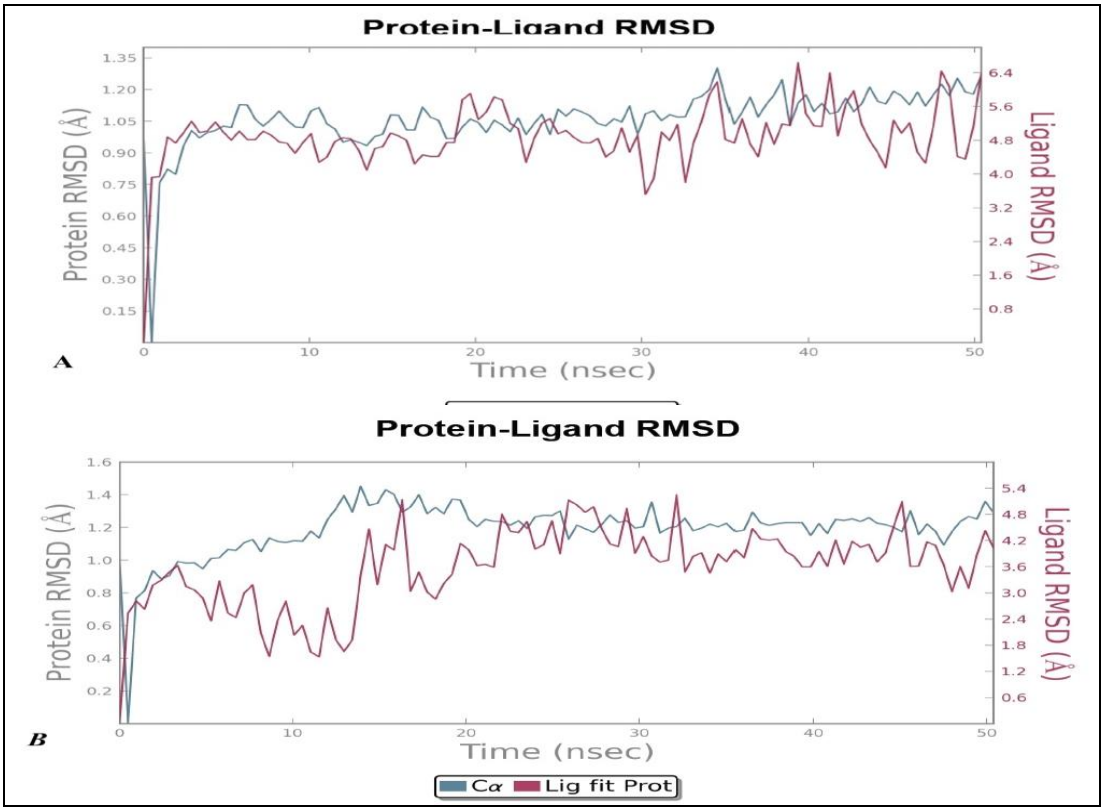

FIG. 10: FIGURE 10A AND 10B SHOWED THE STABILITY OF THE ALOE- EMODIN AND RUTIN WITH RECEPTOR (4MJU) OVER 50 NS SIMULATION PERIOD. AMONG WHICH IT DEPICTED THE RECEPTOR – ALOE EMODIN BEST STABILIZED BETWEEN 22-50 NS WHEREAS THE RECEPTOR – RUTIN BEST STABILIZED AROUND 20-50 NS TIME PERIOD.

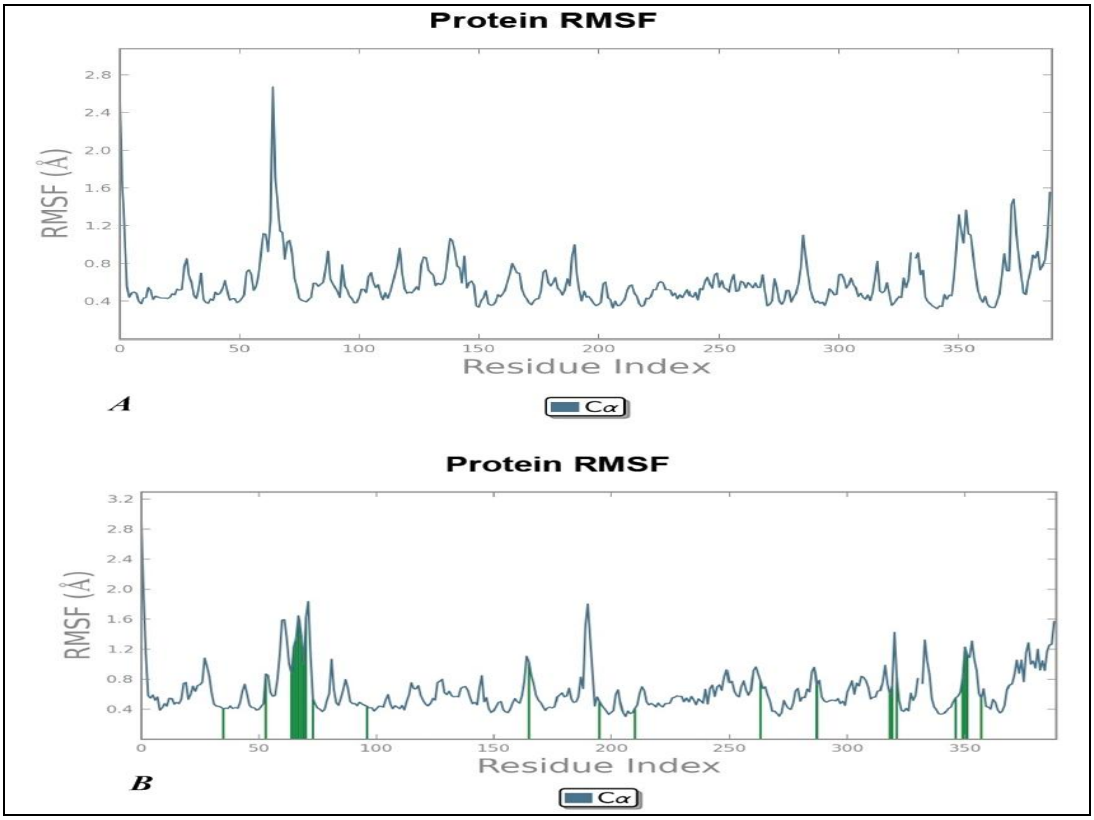

FIG.11: FIGURE 11A AND 11B SHOWS THE ROOT MEAN SQUARE FLUCTUATION OF PROTEIN BACKBONE. FIGURE 8B ALSO SHOWS THAT CORRESPONDING INTERACTION POINTS OF RUTIN FITTED IN RECEPTOR PROTEIN. EVERY SPIKE IN THE RMSF GRAPH DEPICTS ONE INTERACTIVE POINT WITH RESPECT TO ASSOCIATED PROTEIN/ RECEPTOR STRUCTURE.

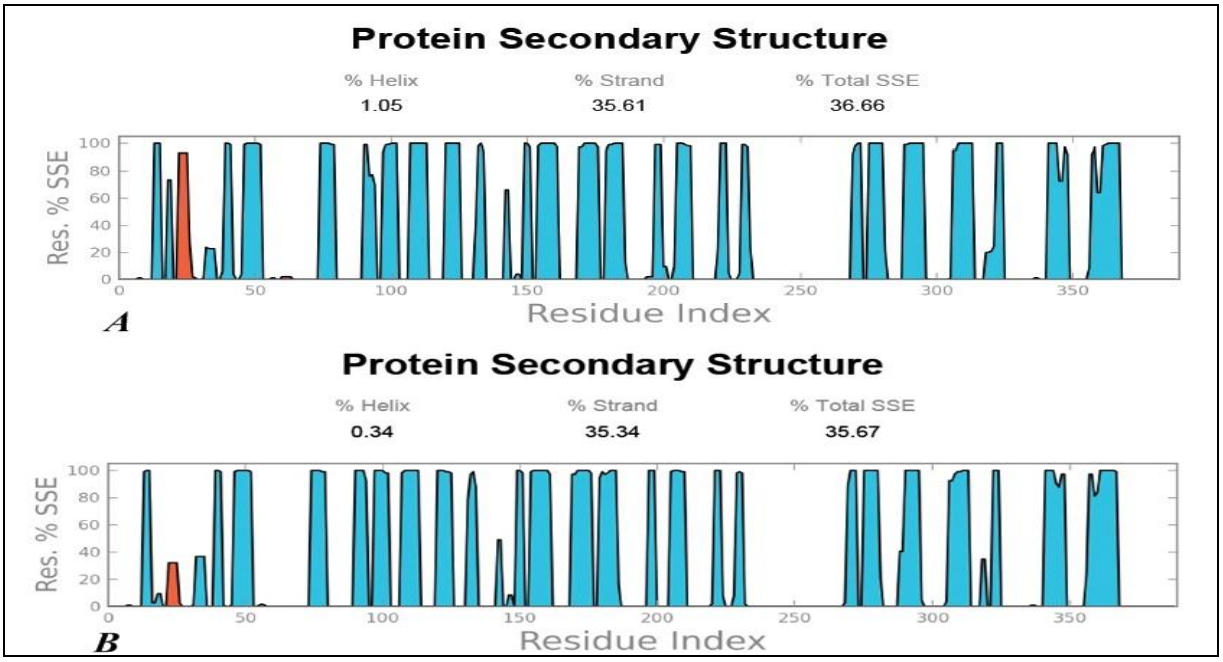

FIG.12: FIGURE 12A AND 12B SHOWS REPORTED SSE DISTRIBUTION BY RESIDUE INDEX THROUGHOUT THE PROTEIN STRUCTURE FOR ALOE EMODIN-NEURAMINIDASE AND RUTIN-NEURAMINIDASE COMPLEXES. COMPLEXES SHOW 1.05% AND 0.36% ALPHA HELIXES INDUCED IN RECEPTOR.

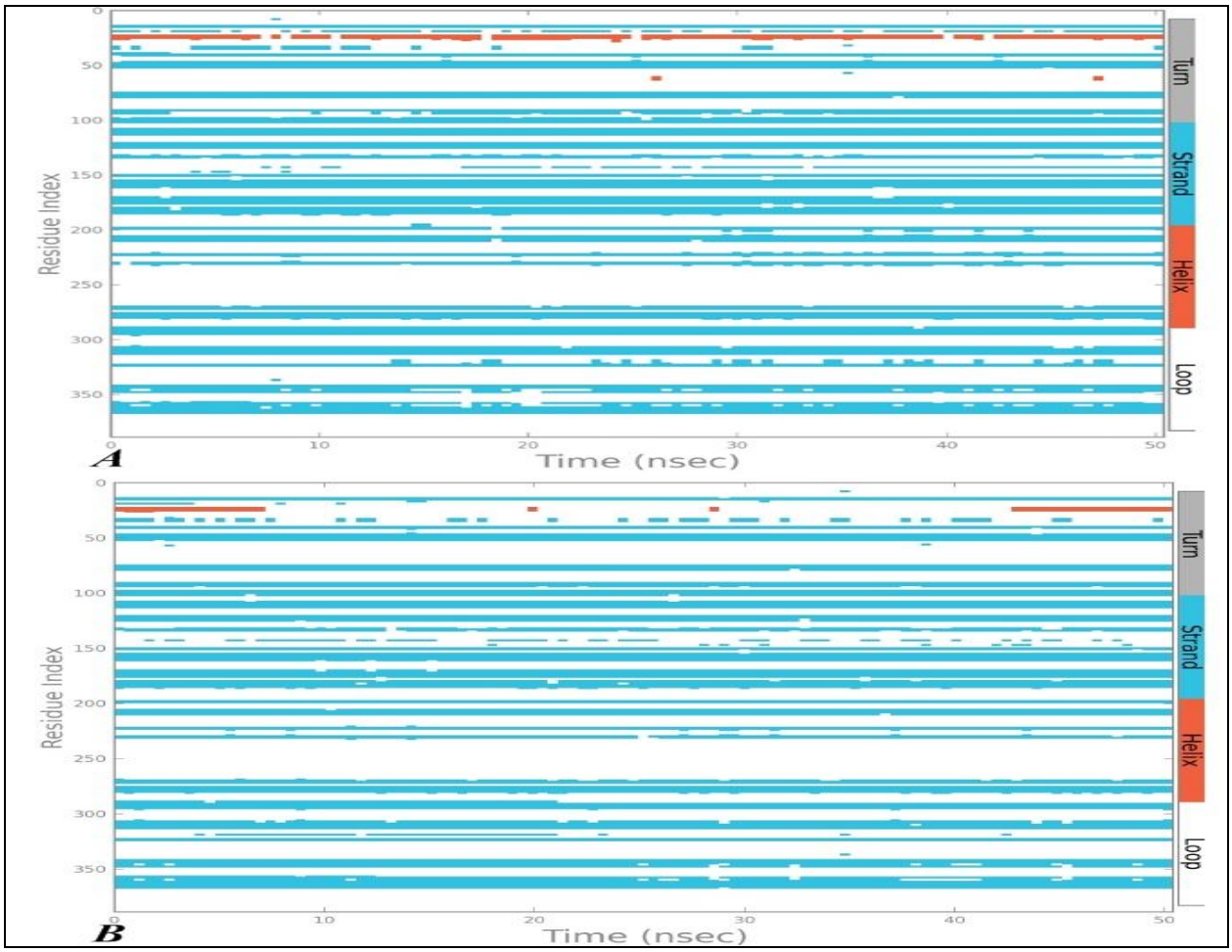

FIG.13: FIGURE 13A AND 13B SHOWS REPORTED SSE DISTRIBUTION BY RESIDUE INDEX THROUGHOUT THE PROTEIN STRUCTURE FOR ALOE EMODIN-NEURAMINIDASE AND RUTIN-NEURAMINIDASE COMPLEXES. COMPLEXES SHOW STABLE CONFORMATIONAL MODIFICATION IN ACTIVE SITE POCKET IN HYDROPHOBIC CORE OF RECEPTOR.

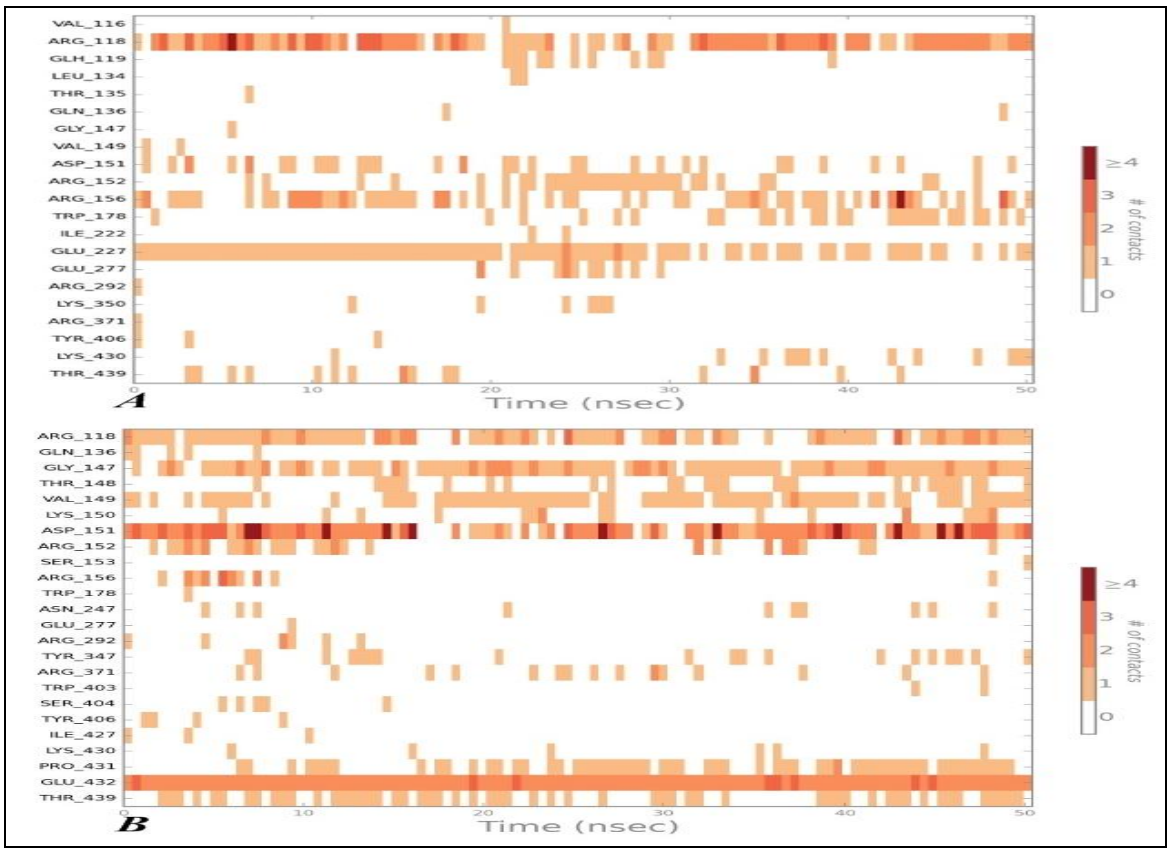

FIG 14: FIG 14A AND 14B SHOWED ALOE EMODIN AND RUTIN RESIDUES INTERACTION WITH THE PROTEIN IN EACH TRAJECTORY FRAME. SOME RESIDUES MADE MORE THAN ONE SPECIFIC CONTACT WITH THE LIGAND, WHICH WAS REPRESENTED BY A DARKER SHADE OF ORANGE, ACCORDING TO THE SCALE TO THE RIGHT OF THE PLOT.

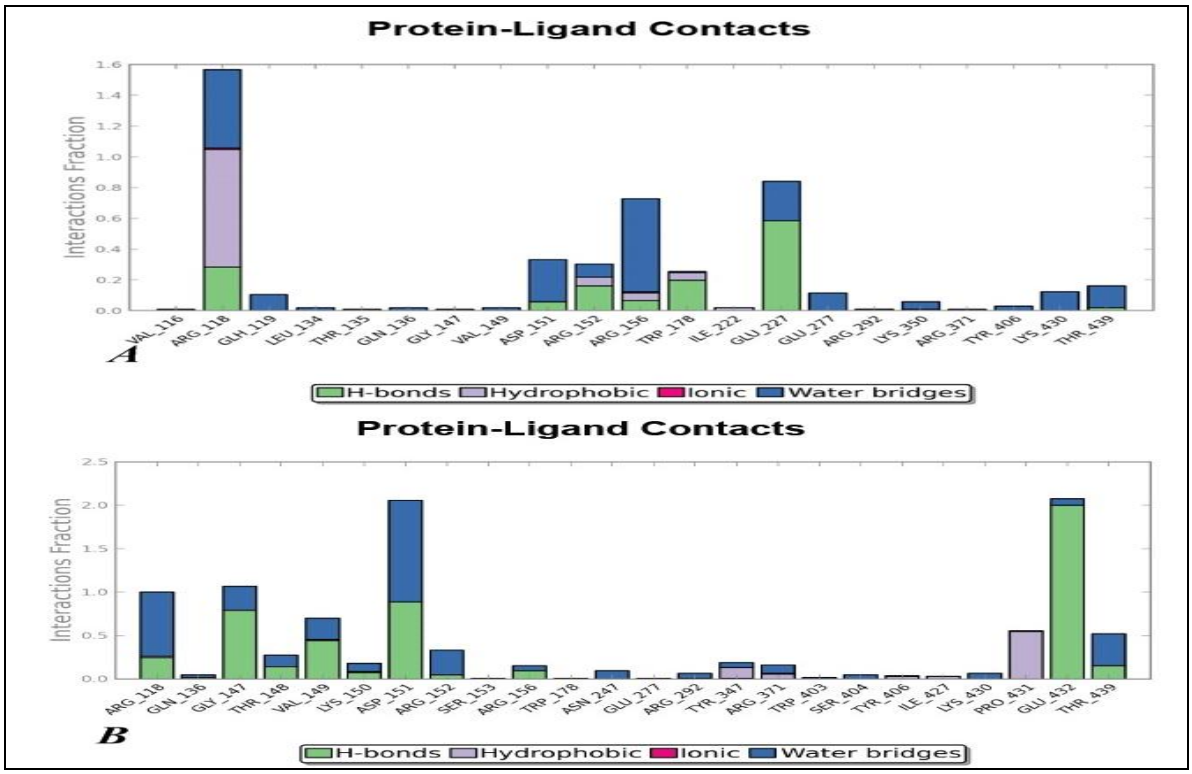

FIG. 15: FIG 15A AND 15B CATEGORIZED INTO FOUR TYPES: HYDROGEN BONDS, HYDROPHOBIC, IONIC AND WATER BRIDGES. THE STACKED BAR CHARTS ARE NORMALIZED OVER THE COURSE OF THE TRAJECTORY: FOR EXAMPLE, A VALUE OF 0.7 SUGGESTS THAT 70% OF THE SIMULATION TIME THE SPECIFIC INTERACTION IS MAINTAINED.

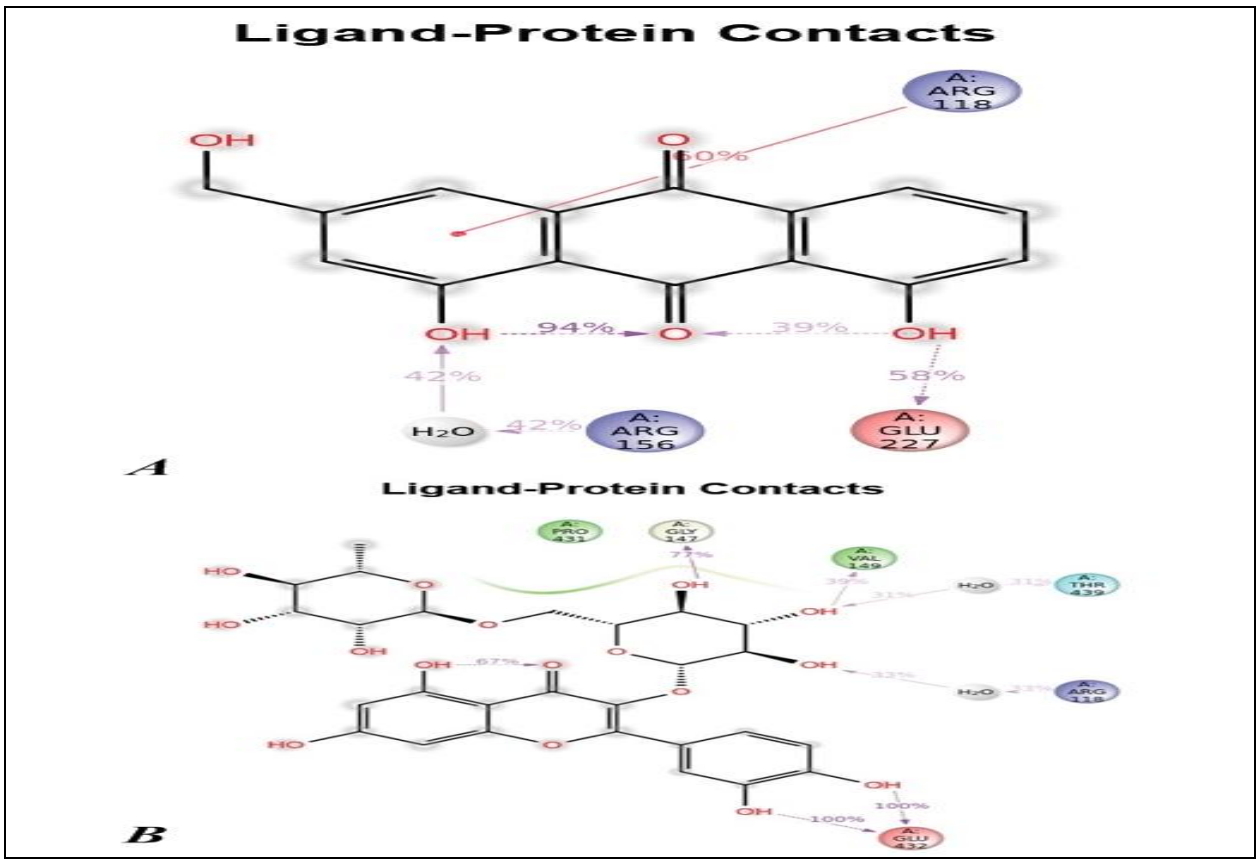

FIG. 16: FIG 16A SHOWS ALOE EMODIN COULD BIND 60% TIME WITH PI CATAION WITH ARG 118 WHEREAS FIG 16B SHOWS RUTIN HAVE BINDING 100% WITH GLU 432 BY HYDROGEN BONDING.

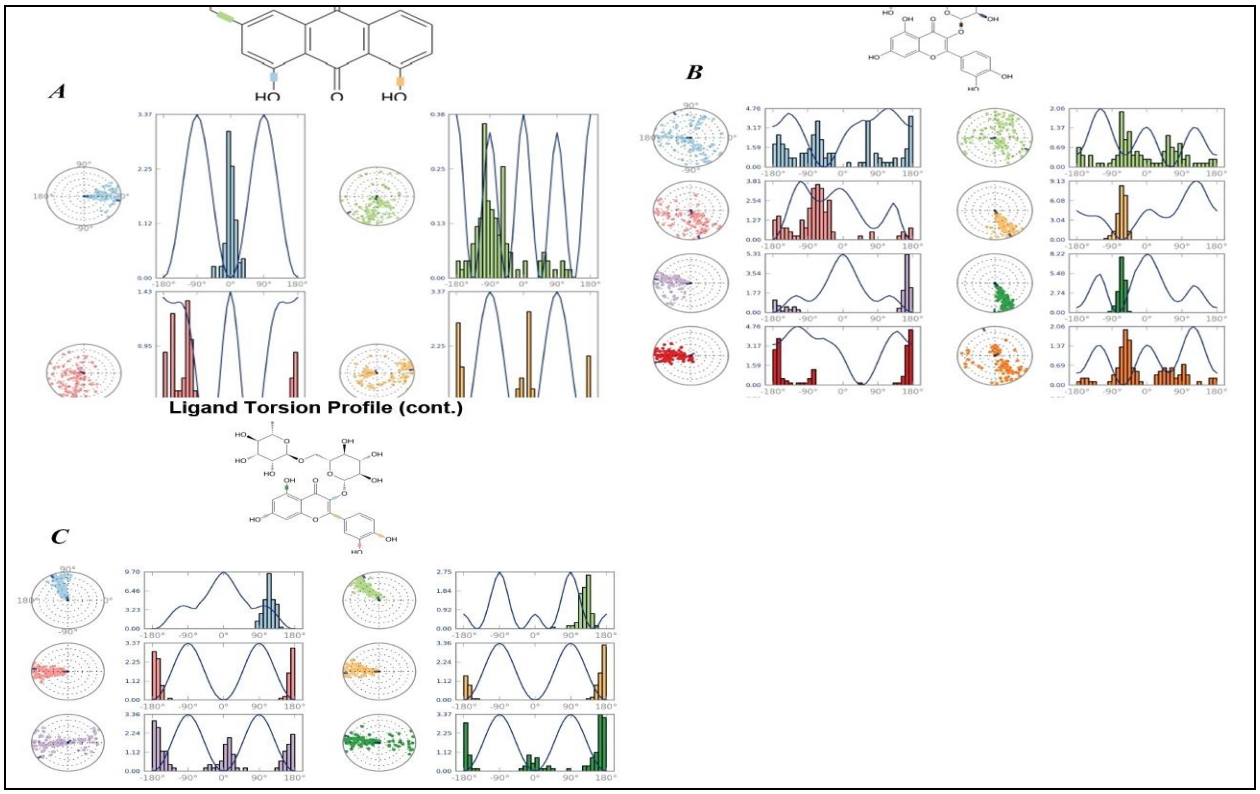

FIG. 17: FIGURE 17 A AND FIGURE 17 B SHOWED THE ALOE EMODIN AND RUTIN TORSIONS PLOT WHICH SUMMARIZED THE CONFORMATIONAL EVOLUTION OF EVERY ROTATABLE BOND (RB) IN THE LIGAND THROUGHOUT THE SIMULATION TRAJECTORY (0.00 THROUGH 50.00 NSEC). THE WIDE RANGE VARIATION ON TORSION ANGLE CONFORMATION ABILITY ATTRIBUTES TO THE FLEXIBILITY OF THE LIGAND.

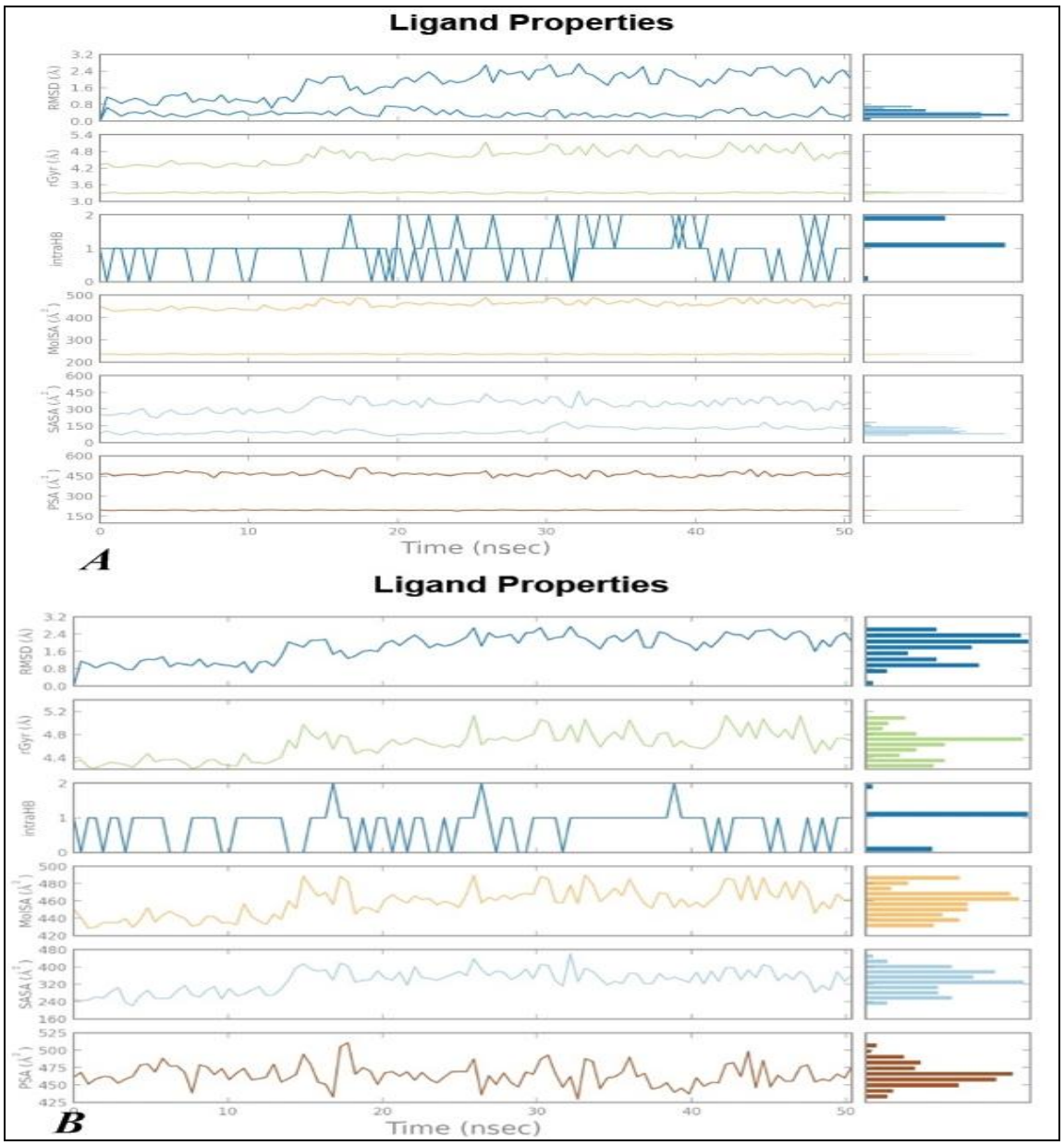

FIG 18: FIGURE 18 A AND FIGURE 18 B SHOWS THE DIFFERENT PROPERTIES OF ALOE EMODIN AND RUTIN. IT SHOWS THE DISTRIBUTION OF ROOT MEAN SQUARE DEVIATION RADIUS OF GYRATION, INTRA MOLECULE HYDROGEN BOND, MOLECULAR SURFACE AREA, SOLVENT ACCESSIBLE SURFACE AREA, II (CARBON AND ATTACHED HYDROGENS) COMPONENTS OF SOLVENT ACCESSIBLE SURFACE AREA,OVER THE 50 NSEC SIMULATION TIME PERIOD.

TABLE 1a: RMSD (A^0) VALUES OF SELF-DOCKING (RED COLOR VALUES) AND CROSS DOCKING CRYSTAL POSE REPRODUCIBILITY FOR THE PROTEINS WITHOUT CONSERVED WATERS. 27S, 2H8, 1SJ, 1SL, 1SN, 1SO AND LNV ARE CO-CRYSTAL LIGANDS OF 4MJU, 4KS1, 4KS2, 4KS3, 4KS4, 4KS5 AND 3TI3 RESPECTIVELY

Identifier/ PDBID	27S	2H8	1SJ	1SL	1SN	1SO	LNV	Average	Average: Open	Average: closed
4MJU	3.313	3.754	6.15	4.181	3.414	5.558	5.839	5.009	4.095	4.981
4KS1	5.924	2.907	2.769	4.626	4.833	5.771	3.476	4.592	5.509	3.44
4KS2	6.06	2.904	2.745	5.189	5.723	5.754	4.682	5.007	5.845	3.88
4KS3	3.31	3.47	2.92	1.788	3.102	7.572	4.031	4.227	4.661	3.052
4KS4	6.209	6.157	3.052	2.511	2.229	3.684	6.117	4.719	4.04	4.459
4KS5	3.537	5.946	6.507	2.71	2.34	3.609	5.904	4.818	3.162	5.266
3TI3	5.792	2.922	2.981	4.489	5.89	6.119	3.654	5.041	5.933	3.511

TABLE 1b: RMSD (A^0) VALUES OF SELF-DOCKING (RED COLOR VALUES) AND CROSS DOCKING CRYSTAL POSE REPRODUCIBILITY FOR THE PROTEINS CONSERVED WATERS.

Identifier/ PDBID	27S	2H8	1SJ	1SL	1SN	ISO	LNV	Average	Average: Open	Average: closed
4MJU	2.132	1.435	0.86	3.353	4.306	7.132	2.419	3.091	4.523	2.016
4KS1	5.627	0.868	0.901	4.791	6.645	7.899	5.819	4.65	6.72	3.094
4KS2	5.742	0.844	0.374	4.919	5.367	6.503	4.081	3.975	5.87	2.554
4KS3	3.358	1.543	1.19	1.903	2.204	7.742	2.679	2.945	4.43	1.828
4KS4	6.244	1.372	0.966	2.212	1.158	1.466	5.927	2.763	2.956	2.619
4KS5	3.399	1.119	1.511	2.798	1.203	1.442	6.047	2.5	2.01	2.868
3TI3	6.118	1.16	1.74	4.568	4.953	4.762	3.536	3.8	5.277	2.751

TABLE 2: THE TABLE SHOWS ENRICHMENT FACTORS (EF), BEDROC AND RIE VALUES OF DOCKING MODELS.

Docking Models	EF(1%)	EF(2%)	EF(5%)	EF(10%)	BEDROC(α=20)	RIE
4MJU	2.1`	1.4	0.55	0.27	0.88	0.48
4KS5	1.8	1.1	0.47	0.24	0.84	0.44
4KS3	1.5	0.9	0.42	0.22	0.80	0.42

TABLE 3: THE TABLE SHOWS % YIELDS OF ACTIVE, % ACTIVES, SENSITIVITY, SPECIFICITY OF DOCKING MODELS. IT SHOWS THAT 4MJU, 4KS5 AND 4KS3 DOCKING MODELS OF CAN GENERATE OF 94.7 %, 91.09 % AND 89.07 % SIMILARITY HIT WITH ACTIVE AND DECOY LIGAND LIBRARY.

Sl no	Docking Model	%Actives	Sensitivity	Specificity	Goodness of Hits (GH score)	% of similarity Hit
1	4MJU	71	0.93	0.86	0.65459	94.7
2	4KS5	69	0.86	0.83	0.59121	91.09
3	4KS3	65	0.82	0.80	0.55215	89.07

TABLE 4: THE TABLE SHOWS 4MJU AND 3TI3 DOCKING MODELS GENERATED DOCKING SCORE OF DIFFERENT PHYTOCHEMICALS LIGAND LIBRARY

Ligand Name	3TI3 Docking Model	4MJU Docking Model
Abetic acid	-2.474	-2.576
Aloe emodin	-8.168	-9.168
Apocynin	-8.472	-8.472
AzadirachtinA	-4.896	-5.896
Berberin	-2.475	-4.475
Betastisterol	-1.51	-5.51
Caryophyllene	-2.324	-6.324
Cinamaldehyde	-2.695	-5.695
Columbin	-3.312	-3.312
Courmaric acid	-7.821	-7.821
Curcumin	-4.576	-4.576
Eugenol	-3.553	-3.553
EuxanthicAcid	-6.163	-6.163
Euxanthicmod1	-8.112	-5.112
Galliac Acid	-7.715	-6.715
Piperin	-3.31	-3.31
Protocatechemic acid	-8.101	-8.101
Rutin	-8.291	-9.791
Shikimic Acid	-7.185	-7.185
Ursolic acid	-7.404	-7.404
Xeronine	-6.772	-6.772
Zanamvir	-7.73	-8.73

TABLE 5: THE TABLE SHOWS SPECIFICITY OF 4MJU AND 3TI3 DOCKING MODELS WITH RESPECT TO DELTA G BINDING AFFINITY WITH TOP DOCKED PHYTOCHEMICALS AND REFERENCE MOLECULES.

Docking Model	Glide Score	$\Delta G_{binding}$	Ligands
4MJU	-9.791	-51.849	Rutin
	-9.168	-50.365	Aloe emodin
	-8.73	-44.085	Zanamvir
	-8.112	-43.871	27S
3TI3	-8.291	-49.765	Rutin
	-8.168	-47.87	Aloe emodin
	-7.73	-40.085	Zanamvir
	-7.712	-44.891	Laminavir

As example, studies with ERBB2+ breast cancer have shown that targeting numerous ancillary kinases expressed in higher concentration by adaptive kinome reprogramming after the development of susceptibility to synergistic effect of curcumin and berberin regime management to growth inhibition of tumor cells variably. Using an extensive high throughput screening we recommend for first time a class of phytochemical neuraminidase inhibitor, validated by several N1 inhibition assays and further characterized by extensive molecular modeling. Our computational approach was based on ligand-based N1 classification models and N1 structure-based models integrated with physicochemical property prediction along with a robust virtual screening method. The N1 classifiers were trained on counted N1 inhibitors against 750 of N1 decoy compounds and the N1structure-based models made use of several available co-crystal structures. It should be distinguished that these models are ranked depending upon its ability to separate compounds by predictive property and these models are probabilistic models too. Models can be quantified by enrichment factor and ROC score (see Results).

The statistics-depending classification of models (or any predictor) therefore should be interpreted as a capability to predict single active compound or a certain percentage of a small sample size. Our high-throughput computational screening pipeline balanced predicted N1 activity with favorable physicochemical properties before applying the neuraminidase structure based model. This prioritized innovative lead-like neuraminidase inhibitors among a big set of compounds and then selecting the most likely N1 binders.

This was a significant challenge, because we were looking at the intersection of phytochemical and chemically synthesized compounds. Two known inhibitors of N1 were included in our ensemble docking protocol; but these compounds did not rank too impressively, supporting our focus on the discovery of novel phytochemical compounds. Our approach is the first to look for natural or nature derived phytochemicals inhibitors using a synergistically performed screening of ligand and structure-based models for each target. As a result of our computational pipeline, we ultimately selected and tested 2 compounds from over 23 shortlisted one. We identified 2 novel N1 binders' phytochemicals, a first-in class compound.

Rutin and Aloe emodin is a potent N1 inhibitor (IC50: 6,11 respectively). To better understand molecular binding interactions of Rutin and Aloe emodin in N1(neuraminidase) and to facilitate future rational optimization, we executed extensive all atom, explicit water MD simulations of these compounds in N1. The 50 ns MD simulation of the predicted N1-Rutin and N1-Aloe emodin complex appeared consistent with the more modest potency observed in the biochemical assays. The observed interactions throughout the duration of the simulation were important hydrophobic pocket motifs for N1. The initial docking pose shows primary interaction with Arg118, a conserved direct positively charged binding residue, through a direct hydrogen bond with the rutin **Fig. 16B** and pi cataion bond with aloe emodin **Fig. 16B**. Binding of Rutin and Aloe emodin appeared to switch between different interactions, but stabilize half way through the simulation with key interactions. Structural analysis of N1 at atomic resolution indicates that Glu 432espouses a closed conformation in the nonexistence of binding.

The binding orientation is the same as zanamivir, oseltamivir, erlotinib, and laminavir inhibitors. Therefore, Rutin and Aloe emodin is a type I neuraminidase inhibitor binding in the active conformation of the activation loop.

The molecular interactions analyzed in the MD simulations suggest possible positions for chemical optimization of Rutin and Aloe emodin to develop derivatives with more equalN1 potency, which would likely escalate compound efficiency. These contain the alkaloid residues and the flavanoid substituent. Such results are also in agreement with the finding by Villar and his groups that AM1 can increase the accuracy in prediction of binding free energies [43]. It gave the impression to be that our strategy is more advantageous due to the number of compounds tested and the eminence of the correlation model. The model showed a reasonable computational cost, and it could be organized for a straightforward application to other groups of molecules with some medical interest. However,

we found that good performance of the collective approach to predict the binding free energy recommends that it can be used to lead discovery and optimization of N1 inhibitor.

Our results do not support or reject the hypothesis that known N1 inhibitors may be privileged viral coating protein binders. We are currently performing analyses to investigate this further. In our method we have established that it is possible to computationally develop such inhibitor compounds. We are presently ranging our selection method to study other important target combinations and we believe that our in-silico method can be comprehensive to discover a variety of novel phytochemical based neuraminidase inhibitors and chemotypes. Here we demonstrated a proof of concept study implementing a pipeline to identify natural derived product based neuraminidase inhibitors. We discovered the first in class phytochemical inhibitor and predict that many dual RNA virus coating protein inhibitors can be identified using this method. We expect this will underwrite to evolving some novel clinical drug leads for the treatment of influenza resistant to current treatment regimens.

ACKNOWLEDGMENTS: We thank Patanjali University for providing the opportunity to undertake this research and thanks to the Patanjali Group for funding the present research. We thank the Schrodinger software team for providing critical input for this research.

REFERENCES:

1. Neumann, Gabriele, Takeshi Noda, and Yoshihiro Kawaoka. "Emergence and pandemic potential of swine-origin H1N1 influenza virus." Nature 2009; 459.7249: 931-939
2. Gubareva, Larisa V., Laurent Kaiser, and Frederick G. Hayden. "Influenza virus neuraminidase inhibitors." The Lancet 2000; 355.9206: 827-835.
3. Pizzorno, Mario Andres. Mechanisms of resistance to neuraminidase inhibitors in influenza A viruses and evaluation of combined antiviral therapy. Diss. Université Laval. 2015
4. Deo, Vipin K., Tatsuya Kato, and Enoch Y. Park. "Chimeric Virus-Like Particles Made Using GAG and M1 Capsid Proteins Providing Dual Drug Delivery and Vaccination Platform." Molecular pharmaceutics 2015; 12.3: 839-845.
5. Kovarik, Katherine Rose, and Joseph E. Kovarik. "Method and System for Prevention and Treatment of Allergic and Inflammatory Diseases." U.S. Patent Application No. 14/574,517.
6. Doyle, Tracey M., et al. "A universal monoclonal antibody protects against all influenza A and B viruses by targeting a highly conserved epitope in the viral neuraminidase." BMC Genomics 2014; 15.Suppl 2: P8.
7. Okomo-Adhiambo, Margaret, Tiffany G. Sheu, and Larisa V. Gubareva. "Assays for monitoring susceptibility of influenza viruses to neuraminidase inhibitors." Influenza and other respiratory viruses 2013; 7.s1:44-49.
8. Moniz, Michelle H., and Richard H. Beigi. "Influenza infection during pregnancy: virology, pathogenesis and clinical challenges." Future Virology 2013; 8.1: 11-23.
9. Kling, Heather M., et al. "Challenges and future in vaccines, drug development, and immune-modulatory therapy." Annals of the American Thoracic Society 2014; 11.Supplement 4: S201-S210.
10. L' Huillier, Arnaud G., et al. "E119D Neuraminidase Mutation Conferring Pan-Resistance to Neuraminidase Inhibitors in an A (H1N1) pdm09 Isolate from a Stem-Cell Transplant Recipient." Journal of Infectious Diseases 2015; 212.11: 1726-1734.
11. Domínguez-Cherit, Guillermo, et al. "Critically ill patients with 2009 influenza A (H1N1) in Mexico." Jama 2009; 302.17: 1880-1887.
12. Jain, Seema, et al. "Hospitalized patients with 2009 H1N1 influenza in the United States, April–June 2009." New England Journal of Medicine 2009; 361.20: 1935-1944.
13. Kato, Kentaro, and Akiko Ishiwa. "The role of carbohydrates in infection strategies of enteric pathogens." Tropical medicine and health 2009; 43.1: 41.
14. vonItzstein, Mark. "The war against influenza: discovery and development of sialidase inhibitors." Nature reviews Drug discovery 2007; 6.12: 967-974.
15. Russell, Rupert J., et al. "The structure of H5N1 avian influenza neuraminidase suggests new opportunities for drug design." Nature 2006; 443.7107: 45-49.
16. Collins, Patrick J., et al. "Crystal structures of oseltamivir-resistant influenza virus neuraminidase mutants." Nature 2008; 453.7199: 1258-1261.
17. Collins, P. J., et al. "Structural basis for oseltamivir resistance of influenza viruses." Vaccine 2009; 27.45: 6317-6323.
18. Gubareva, Larisa V., et al. "Selection of influenza virus mutants in experimentally infected volunteers treated with oseltamivir." Journal of Infectious Diseases 2001; 183.4: 523-531.
19. Lackenby, A., et al. "Emergence of resistance to oseltamivir among influenza A (H1N1) viruses in Europe." Euro surveillance: bulletin europeensur les maladies transmissibles= European communicable disease bulletin13.5.2008
20. Mc Kimm-Breschkin and Jennifer L. "Influenza neuraminidase inhibitors: antiviral action and mechanisms of resistance." Influenza and other respiratory viruses 2013; 7.s1: 25-36.
21. Gubareva, Larisa V. "Molecular mechanisms of influenza virus resistance to neuraminidase inhibitors." Virus research 2004; 103.1: 199-203.
22. López-Causapé, Carla, et al. "The problems of antibiotic resistance in cystic fibrosis and solutions." Expert review of respiratory medicine 2015; 9.1: 73-88.
23. Sastry, G.M.; et al., "Protein and ligand preparation: Parameters, protocols, and influence on virtual screening enrichments," J. Comput. Aid. Mol. Des., 2013; 27(3), 221-234.
24. Jacobson, M. P.; et al, "A Hierarchical Approach to All-Atom Protein Loop Prediction," Proteins: Structure, Function and Bioinformatics, 2004; *55*, 351-367.

25. Jacobson, M. P.; et al, "On the Role of Crystal Packing Forces in Determining Protein Sidechain Conformations," J. Mol. Biol., 2002; 320, 597-608.
26. Mysinger, Michael M., et al. "Directory of useful decoys, enhanced (DUD-E): better ligands and decoys for better benchmarking." Journal of medicinal chemistry 2012; 55.14: 6582-6594.
27. Huang, et al. "Benchmarking sets for molecular docking." Journal of medicinal chemistry 2006; 49.23: 6789-6801.
28. Friesner, et al, "Extra Precision Glide: Docking and Scoring Incorporating a Model of Hydrophobic Enclosure for Protein-Ligand Complexes," J. Med. Chem., 2006; 49, 6177–6196
29. Halgren, T. A.; et al, "Glide: A New Approach for Rapid, Accurate Docking and Scoring. 2. Enrichment Factors in Database Screening," J. Med. Chem. 2004; 47, 1750–1759.
30. Friesner, R. A.; et al., "Glide: A New Approach for Rapid, Accurate Docking and Scoring. 1. Method and Assessment of Docking Accuracy," J. Med. Chem., 2004; 47, 1739–1749.
31. Hariharan, R. et al. Multimcs: a fast algorithm for the maximum common substructure problem on multiple molecules. J. Chem.Inf. Model. 2011; 51, 788–806.
32. Shivakumar, D.; et al, "Prediction of Absolute Solvation Free Energies using Molecular Dynamics Free Energy Perturbation and the OPLS Force Field," *J. Chem. Theory Comput.*, 2010; *6*, 1509–1519.
33. Guo, Z.; et al, "Probing the α-Helical Structural Stability of Stapled p53 Peptides: Molecular Dynamics Simulations and Analysis," Chem. Biol. Drug Des., 2010; 75, 348-359.
34. Kevin J. Bowers, et al, "Scalable Algorithms for Molecular Dynamics Simulations on Commodity Clusters," proceedings of the acm/ieee conference on supercomputing (sc06), tampa, florida, 2006; November 11-17.
35. Kaminski GA, et al: Evaluation and Reparametrization of the OPLS-AA Force Field for Proteins via Comparison with Accurate Quantum Chemical Calculations on Peptides. J Phys Chem B. 2001; 105 (28): 6474-6487.
36. Jorgensen WL, et al Development and Testing of the OPLS All-Atom Force Field on Conformational Energetics and Properties of Organic Liquids. J Am Chem Soc. 1996; 118 (45): 11225-11236.
37. Lyne PD, et al. Accurate prediction of the relative potencies of members of a series of kinase inhibitors using molecular docking and MM-GBSA scoring. J Med Chem. 2006; 49 (16): 4805-4808.
38. Friesner, R. A.; et al. Glide: a new approach for rapid, accurate docking and scoring. 1. Method and assessment of docking accuracy. J. Med. Chem. 2004; 47, 1739−1749.
39. Halgren, T. A.; et al. Glide: a new approach for rapid, accurate docking and scoring. 2. Enrichment factors in database screening. J. Med. Chem. 2004; 47, 1750−1759.
40. Friesner, R. A.; et al Extra precision glide: docking and scoring incorporating a model of hydrophobic enclosure for protein−ligand complexes. J. Med. Chem.49, 2006; 6177−6196.
41. Sherman, W.; et al Novel procedure for modeling ligand/receptor induced fit effects. J. Med. Chem. 49, 534 −553.
42. Sherman, W.; et al. Use of an induced fit receptor structure in virtual screening. Chem. Biol. Drug Des. 2006; 67, 83 −84.
43. Villar R., et al. Are AM1 ligand-protein binding enthalpies good enough for use in the rational design of new drugs? J Comput Chem; 2005; 26: 1347-1358.
44. Mukherjee, Pulok K., and Atul Wahile. "Integrated approaches towards drug development from Ayurveda and other Indian system of medicines." Journal of ethnopharmacology 2006; 103.1: 25-35.
45. Srimad Bagbhatta Ashtanga Hridyam, vidyotini bhasha tika. 1981
46. Vaidyanath Ashtanga Samgriha Sutrasthana, Ayurveda Bhawan Ltd Allahabad. 1981
47. Gorakhnath Chaturvedi and Chaukambha Bhati Charak Samhita of Agnivesha Hindi commentary, Academy, Varanasi, 12th Ed. 1984
48. Bhaskara Govinda, Ghanekar, motile Banarasi Das (Sashruta Samhita Varanasi Reprint. 1981

How to cite this article:
Acharya B, Ghosh S and Manikyam HK: Nature's Response to Influenza: A High Throughput Screening Strategy of Ayurvedic Medicinal Phytochemicals. Int J Pharm Sci Res 2016; 7(6): 2699-19.doi: 10.13040/IJPSR.0975-8232.7(6).2699-19.

All © 2013 are reserved by International Journal of Pharmaceutical Sciences and Research. This Journal licensed under a Creative Commons Attribution-NonCommercial-ShareAlike 3.0 Unported License.

This article can be downloaded to **ANDROID OS** based mobile. Scan QR Code using Code/Bar Scanner from your mobile. (Scanners are available on Google Playstore)